

**Drought and wildfire severity and trend in Los Angeles County:
Recovery-disturbance monitoring and analysis**

YOUNG JUN JEONG

Introduction

This project studies the patterns and intensity of wildfires and droughts, with a focus on the vulnerability of California, United States. California has been plagued by frequent and severe environmental disasters including those mentioned above in the past decade. In addition, common weather patterns have been altered due to ongoing climate change, resulting in the formation of an event characterized by low precipitation as well as extremely high temperatures (AghaKouchak et al., 2014). The wildfires lay waste to California's ecosystem through the loss of both biomass and water body volume. The droughts both destroy plants and help create wildfires. Some of the questions this project aims to answer are: "Why are these wildfires and droughts happening at a more intense rate?", "What impacts do wildfires and droughts have on the environment and its surrounding area?" and "What are the possible solutions to these current problems?". We are going to study how areas impacted by drought have changed over time as well as compare them with other similar areas. Rather than examining California in its entirety, this study focuses on a specific section of the state to ensure greater focus and precision. The project examines changes in the affected areas over time and compares the impact on different regions. This approach allows for a more focused and comprehensive analysis while mitigating potential limitations associated with studying a broader geographic area.

The importance of the topic can be explained by the substantial population and its impacts. California contains a population of over 39 million inhabitants. The wildfires and droughts have significant repercussions on many individuals' lives, leading to their displacement from affected areas. Wildfires produce harmful air pollutants that could cause cancer and increase the risk of heart attacks. 15 of the 20 largest wildfires in California history have occurred since the year 2000. In addition, ten of the most expensive and destructive fires have taken place since 2015 (Stephens et al, 2018). High severity to extreme fires can hamper the ability of an ecosystem to recover. The droughts affect wildlife as well. Furthermore, drought can have adverse negative economic impacts. According to the state of California in 2021-2022, agricultural losses from the drought have caused a loss of 3.5 billion dollars in California's food processing and manufacturing industries, taking 12 000 agricultural jobs along with it. During California's 2015 drought, people were asked to reduce their water use by 25% statewide, (Di Baldassarre et al, 2018). Their quality of life has lowered because of the drought.

Prior to conducting this study, the project team possessed some knowledge about the subject matter and was aware of recent wildfires and droughts in California, having seen various clips and videos of the

wildfires on social media. The effects of the wildfires were already known, such as the destruction of wildlife and the displacement of animals. The wildfires are likely becoming more intensified due to global warming. Furthermore, the project team knew that the droughts in California may intensify progressively. California is home to many farms, known as the largest producers and exporters of almonds, and it was a safe assumption that they are likely to be negatively affected by the drought. California was probably forced to import water resources from outside. Another piece of information that was known before doing this study was that California has been hit by multiple droughts.

This study may advance the knowledge of the situation, one of its key goals. Using different satellite images and data which are to be observed from different years for comparison, the study advances the knowledge of how wildfires and droughts affect the vegetation of the impacted areas, the intensity of the impact and the change over time by study region. The analysis uses data, including time-series biomass vigour, soil support, and vegetation moisture content, to examine the disturbances and recoveries on agricultural lands or forests in Los Angeles County. This study aims to contribute to the development of potential solutions for mitigating the impacts of wildfires and droughts in California.

Methodology

The features being studied in this project are the vegetation areas in Los Angeles County, composed of mountainous terrains and agricultural lands. These areas include but are not limited to Santa Monica Mountains, San Gabriel Mountains, and Sierra Madre Mountains. The study site was selected based on its proximity to the urban interface as well as its ecological significance as a transition zone between the chaparral and oak woodland ecosystems. The study site is located at $34^{\circ} 3' N$ $118^{\circ} 15' W$ with a total area of coverage of $12,310 \text{ km}^2$ (see Figure A.1). Barren lands/wastelands exist on the borderlines of the vegetation and urban areas.

In order to capture the effects of wildfires and droughts in the area of the study over the recent decade, specifically 2014 - 2022, the project uses a combination of Landsat 8 Operational Land Imager (OLI) images. These images were collected with a preference towards both containing the least in-land cloud cover and possessing image acquisition dates in July or close to July (see Table A.1). Each satellite raster image is used to calculate various required spectral indices such as Normalised Difference Vegetation Index (NDVI) for general biomass vigour, Normalised Burn Ratio (NBR) for burn ratio of the area, and Land Surface Water Index (LSWI) for soil and in-vegetation moisture content (see Table A.2). These indices provide the visual context of year-to-year changes in volume loss of biomass and moisture content.

Classification of Land Cover Land Use (LULC) is processed through the use of an unsupervised classification algorithm in ERDAS Imagine, a remote sensing software package. This allows the non-urban area classes (mountainous vegetation, residential vegetation, agricultural lands, water, etc.) and urban area classes to be detected and merged as a binary output. This is necessary such that the detected urban area can be used as a polygon shapefile mask for the visual effect of highlighting the aforementioned vegetation areas of Los Angeles County. Among the nine different dates of image acquisition, the false colour composite image of 2022 was selected as the common highlighting mask layer (see Figure B.1), despite its lower overall accuracy of 78.00% and a moderate level of agreement (as indicated by kappa statistic, 0.5066; see Table B.1). This image was chosen because it contained the least amount of classification bias. In previous years' classified images, mountainous regions are mistakenly identified as urban areas. However, this error was not detected in accuracy assessments because of limited random sampling. Therefore, the consistency of visual interpretation of spectral index change, year to year, can be ensured by using a single mask layer over all years of data acquisition with minimum bias.

To create a multidimensional raster layer, Landsat 8 OLI image packages are stacked in a time-chronological sequence. This multidimensional raster layer is used as the input for the multitemporal change detection of spectral indices and corresponding Digital Numbers (DN) of the Landsat 8 bands including Red, Near-Infrared (NIR), and Shortwave Infrared (SWIR-1 and SWIR-2). Sensitivity change by the photosynthetic condition of vegetation, presence of water content, and charred material are represented as repetitive disturbances and recoveries. These index results can be visualized on the Pixel Time Series Change Explorer using the desktop Geographical Information Systems (GIS) software application, ArcGIS Pro. They will take the form of a segmented plot of the observations and trends. Landsat-based Detection of Trends in Disturbance and Recovery (LandTrendr) is used to fit the trend line of the observed DN values. As LandTrendr was developed for multitemporal satellite data, it takes in pixel values as input data and analyses them through the use of regression models to capture, label and map the changes (Toker et al., 2021). The temporal profile interface of the historical DN values along with the fitted trend models by LandTrendr partitions disturbances and recoveries as pairs of one date of acquisition to another date of acquisition. This allows for the overall disturbance to be rasterized as Differenced Spectral Index (DSI), the pixel change in spectral index value from the previous date. In this scenario, DSI is represented by the pre-fire/drought year to the post-fire/drought year. Hence, the DSI for each of our three spectral indices is dNDVI, dLSWI, and dNBR, respectively. Each DSI is distributed by order of the steepness of segment slopes for averaging. This is performed in such a way that the visualization of frequently disturbed areas is adjusted to be prioritized and emphasized in terms of the level of loss in biomass vigour and water content along with burn damage severity, and the significant consequences of wildfires and droughts.

Results

The NDVI for the maps between 2014 - 2016 shows a relatively consistent NDVI value with only a slight decrease from 2014 to 2015 followed by an increase again in 2016. 2017- 2019 are years of growth with NDVI values increasing. 2020 experienced peak NDVI growth, followed quickly by a sudden decline in 2021. Finally, 2022 experienced another year of growth.

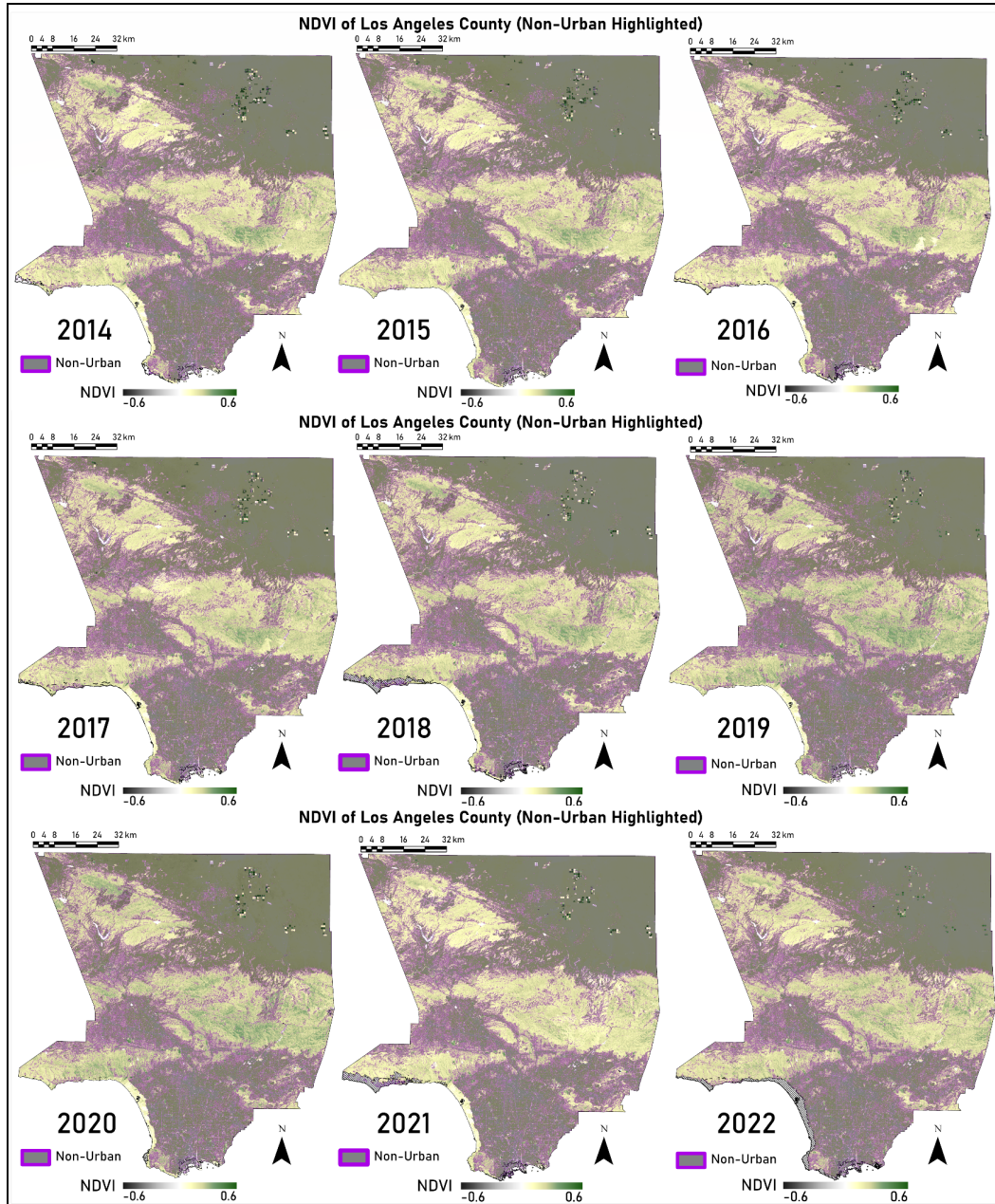


Figure 1. Map of Normalised Difference Vegetation Index Maps by Year (Non-Urban Highlighted)

Note. Landsat-8 OLI July of 2014, 2015, 2016, 2017, 2018, 2019, 2020, 2021 2022

Band 4 (Red) and Band 5 (NIR) Arithmetic

The results between 2014 - 2016 show a relatively consistent LWSI value with only a slight decrease each year. 2017- 2019 are years of growth with LWSI values increasing, 2019 being the peak in the growth. A slight decline in 2020 was followed quickly by a sudden decline in 2021. Finally, 2022 experienced another year of slight growth.

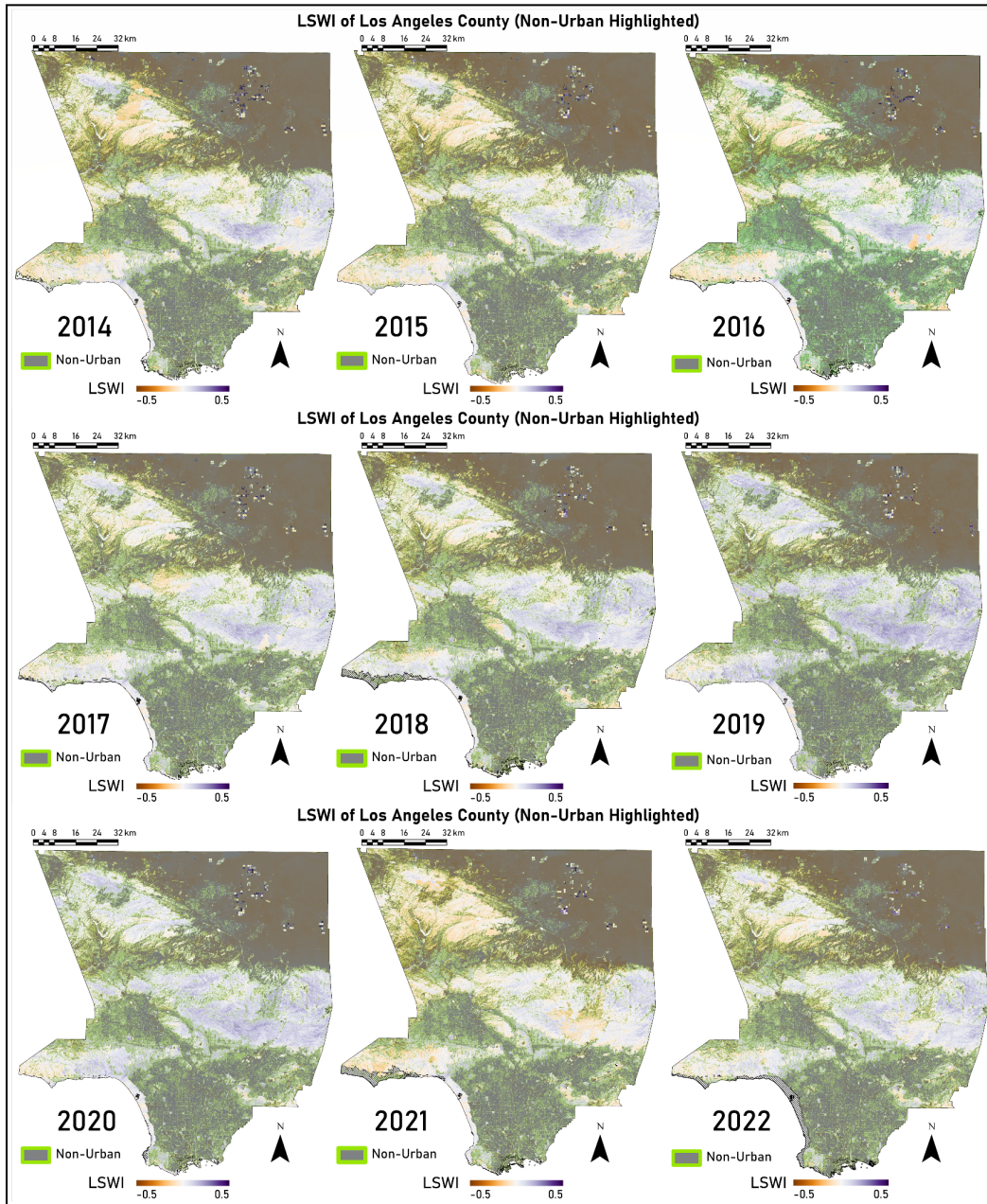


Figure 2. Map of Land Surface Water Index by Year (Non-Urban Highlighted)

Note. Landsat-8 OLI; July of 2014, 2015, 2016, 2017, 2018, 2019, 2020, 2021, 2022

Band 5 (NIR) & Band 6 (SWIR-1) Arithmetic

From July 2014 to 2016, a moderate-sized area regrew while smaller patches of land experienced low severity. These smaller patches regrew from July 2016 to July 2017, while another area experienced low severity, this time covering more land. From July 2017 to July 2018, the previous area regrew while many smaller areas experienced low severity. The range of time with the most changes was July 2020 to July 2021 where two large areas experienced low to moderate severity along with many smaller areas.

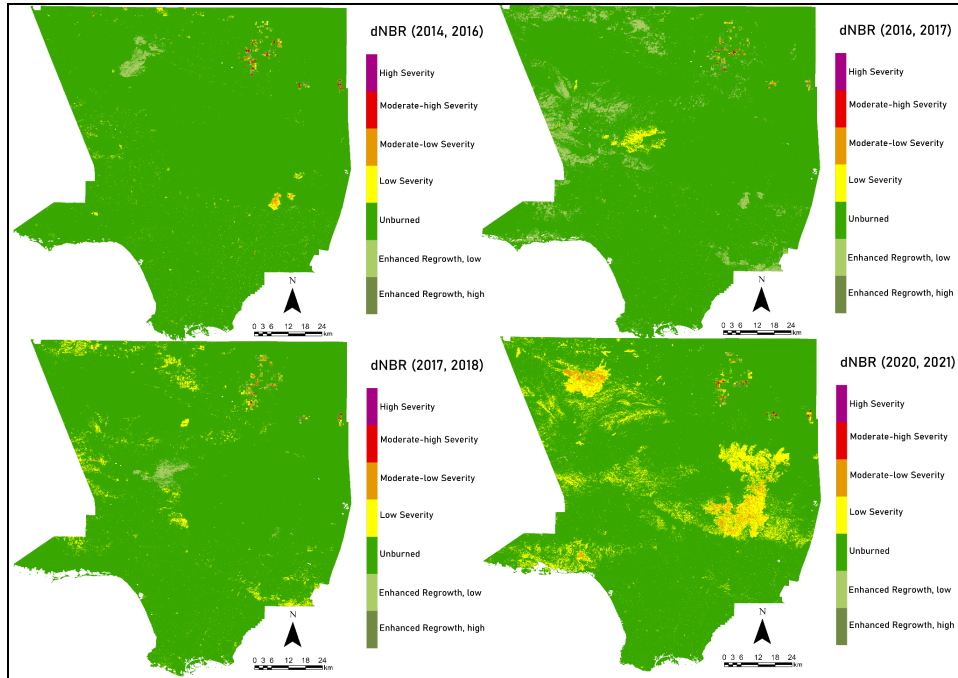


Figure 3. Map of dNBR by Major Observed Value Disturbance Segments

Note. Landsat-8 OLI; July of 2014, 2016, 2017, 2018, 2020, 2021
Band 5 (NIR) and Band 7 (SWIR-2) Arithmetic

Observing the map we can see a trend happening over time from 2016-2022. Some areas were regrowing in 2016 that ended up being classified as low severity in 2022. A large remainder of the study area was unburned from 2016-2022.

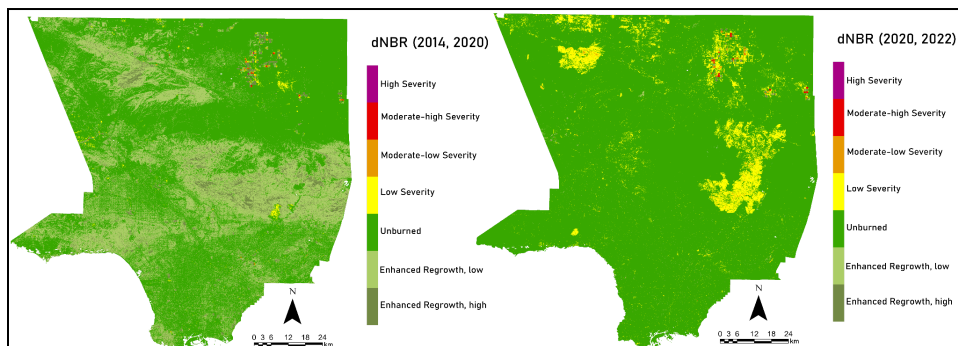


Figure 4. Map of dNBR by Overall Disturbance Trend Segments

Note. Landsat-8 OLI; July of 2014, 2020, 2020, 2021
Band 5 (NIR) and Band 7 (SWIR-2) Arithmetic

On the temporal file of each spectral index and band of interest plotted and fitted using the LandTrendr method, NIR DN had two major disturbances in July 2014-2015 and 2020-2021. Recovery could be observed during July 2015-2018 and growth during July 2018-2020 (see Figure 5(a)). SWIR-1 DN displayed minor disturbances and recoveries from 2014-2020 but increased significantly from July 2020 to July 2021 before levelling down in 2022 (see Figure 5(b)). SWIR-2 DN had two major disturbances in July 2017-2018 and 2020-2021 (see Figure 5(c)). NDVI showed three significant disturbance periods: 2014-2016, 2017-2018, and a notable decline in 2020-2021. (see Figure 5(d)). LSWI exhibited the same disturbance periods as NDVI with steeper slopes (see Figure 5(e)). NBR had a minor disturbance during 2014-2016 and a major disturbance period during 2017-2018 and 2020-2021 (see Figure 5(f)).

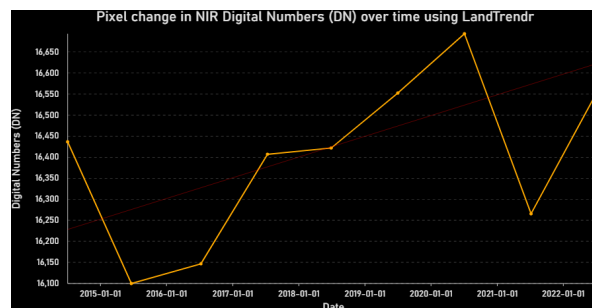


Figure 5(a). Temporal Profile: NIR DN

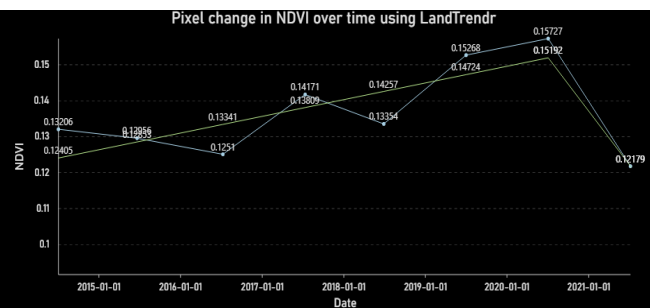


Figure 5(d). Temporal Profile: NDVI Pixel Value

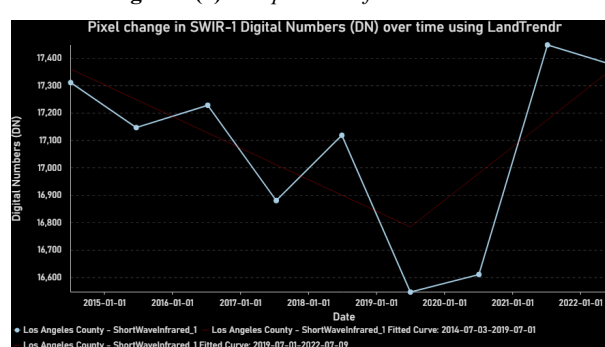


Figure 5(b). Temporal Profile: SWIR-1 DN

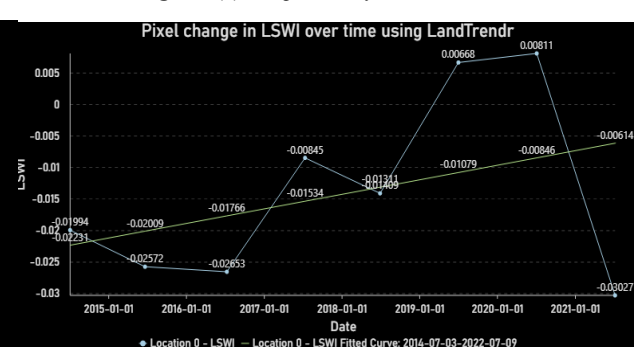


Figure 5(e). Temporal Profile: LSWI Pixel Value

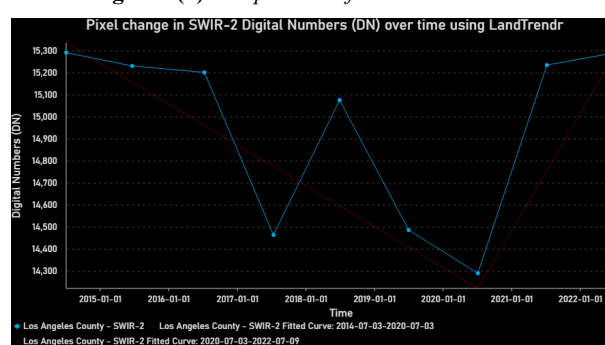


Figure 5(c). Temporal Profile: SWIR-2 DN

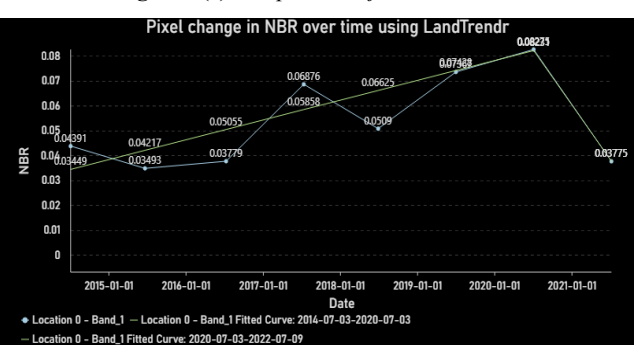


Figure 5(f). Temporal Profile: NBR Pixel Value

Figure 5. Temporal Profile of Digital Numbers (DN) and Pixel Values over Time using LandTrendr

The weighted average of the Difference Spectral Indices examined: dNDVI, dLSWI, and dNBR are displayed as a binary output where the raster cells coloured in red are the pixels having their values belonging to the highest weighted average Difference Spectral Index value class based on natural break classification, and the raster cells displayed in black are the rest of the values less than the minimum threshold of the highest class for each Difference Spectral Index.

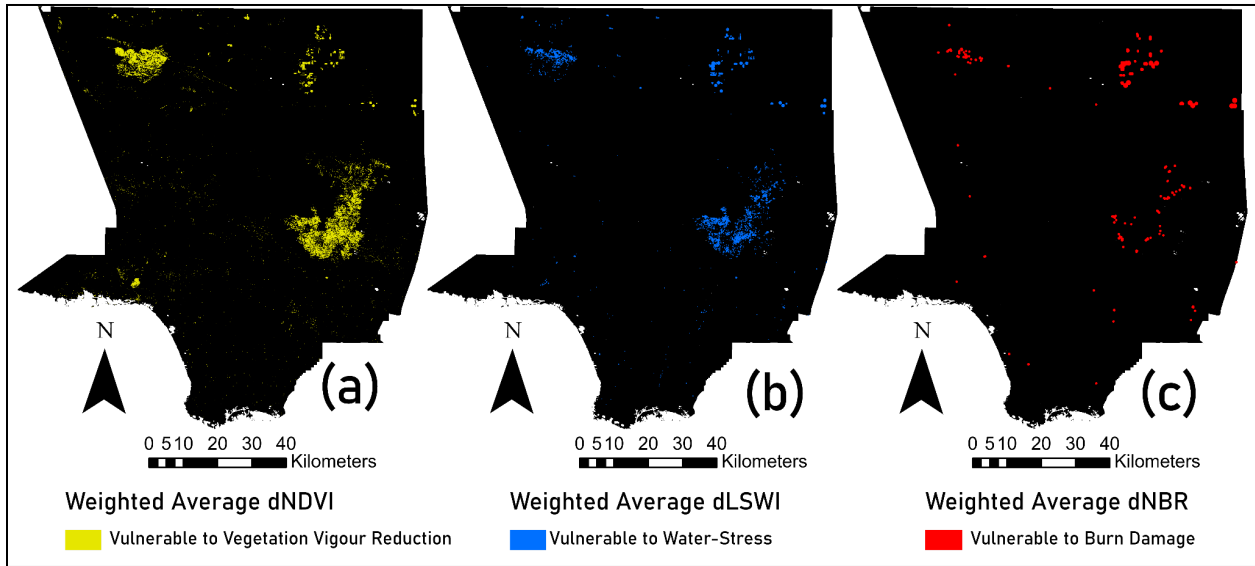


Figure 6. Areas Vulnerable to (a) Vegetation Vigour Reduction, (b) Water Stress, and (c) Burn Damage

Note. Landsat-8 OLI Multidimensional Stack of 2014, 2015, 2016, 2017, 2018, 2019, 2020, 2021, 2022

Band 4 (Red), Band 5 (NIR), Band 6 (SWIR-1), Band 7 (SWIR-2) Arithmetic

Discussion

The temporal profile of the digital numbers of each spectral band of multidimensionally stacked Landsat-8 images displays the observed values in a fitted trend of disturbance and recovery. On an annual scale, from the NIR DN temporal profile, which is sensitive to biomass vigour, we can identify possible periods of loss and growth of photosynthetic health levels of the mountainous and agricultural vegetations of Los Angeles County based on the disturbance segments introduced above. SWIR-1 is very sensitive to moisture, therefore, it can be used for indicating the level of soil moisture and vegetation in the image, hence can notice that loss or absence of water content in 2019 on the overall trend, indicating drought and possibly wildfire. For SWIR-2 which is particularly sensitive to the presence of charred material because it has a strong absorption feature in this spectral region, a general degree of burn damage based on the affected area difference by each discovery and disturbance segment with the potential temporal interval of the wildfire cases over the decade could be predicted (see Figure 5(a), Figure 5(b), and Figure 5(c)).

Furthermore, based on the comparison of the behaviour and trend of DN values of each band but also for the spectral indices, the predictions that were made are found to be partially correct. While wildfires are prevalent, they are not as common as originally projected. Referring to the change in NDVI pixel values over time, the overall trend showed many years of growth or a slight decline in vegetation growth. This is consistent for many of the maps. However, 2020-2021 shows a large decline in vegetation growth due to the record-breaking amount of fires in 2020, which can be seen in our 2020-2021 dNBR map. Approximately 9 917 fires burned 4397809 acres of land over the year. Notably, 2020-2021 was a year of severe drought. Past years with low LSWI values correlated with low NDVI values. This trend can be seen when observing the 2021 LSWI and NDVI maps, where extremely low values were present among both maps. Considering these results, could the California government be more prepared? One method could involve running a much more intensive analysis of current/future water levels. Additionally, they can better prepare themselves by investing in wildfire prevention and increasing water sources for farmers and vegetation in the area (see Figure 5(a), Figure 5(b), and Figure 5(c)).

The disturbance segment intervals identified through analysis of the DN and pixel value trends are used as weight coefficients to calculate the weighted average Difference Spectral Indices. These indices are then used to identify vulnerable regions, high intensity in a shorter period is prioritised, for each type of disaster, including droughts and wildfires. The vulnerability map corresponding to each spectral index shares some parts of its region with another vulnerability map or with all the rest of the vulnerability map. In this case, the shared region of frequent vegetation loss and water stress in high severity can be

interpreted as a drought-vulnerable region and the shared region of frequent vegetation loss, water stress, and burn damage in high intensity can be wildfire & drought-vulnerable regions (see Figure 6).

Despite the conclusive results obtained from the analysis, the project encountered constraints that limited the depth and accuracy of the findings. Although the Landsat-8 images are known as preprocessed for georeferencing, the project only analyses Digital Number values as opposed to actual Surface Reflectance values. This is due to the extensive extra calculations involved for proper atmospheric correction. The urban area mask layer used for highlighting the vegetation areas (see Figure B.1) considers only a single Landsat-8 image, July 2022. Urban region masks for each year could not be used to exclusively extract non-urban regions due to the complex landscapes within Los Angeles County, particularly the borderlines of the mountainous region and urban region. This area has a mixture of barren lands, bare soils, and wastelands, increasing the chances of the Mixed Pixel Problem. This problem occurs when a pixel contains more than one class, causing the image to display a one-digit number, the average of multiple features. As a response, different satellite images with higher spatial resolutions could have been considered. Enhancement of classification accuracy of the urban areas by each year and the creation of masks. Better quality of surface reflectance noise removals of the areas such as urban regions, wastelands, or barren lands, hence extraction of non-urban regions and precise spatiotemporal analysis on the focused areas could be performed, disregarding the urban change or development near the focused study region by each year.

Conclusion

In conclusion, observance and analysis of the patterns of disturbance and recovery in vegetation vigour, water stress and burn damage using the spectral bands and indices that are sensitive to each of the crises were performed, on the multidimensionally stacked Landsat-8 OLI images over the past decade. After catching the disturbance vertices which indicate the temporal interval of each environmental disaster studied, Difference Spectral Indices were evaluated, then weighted averaged for the identification of the frequent vegetation loss, water stress, and Burn Damage occurring, hence vulnerable regions. The common regions of vulnerability maps of vegetation vigour reduction and water stress are found in drought-vulnerable regions and the common regions of all three vulnerability maps are found in wildfire and drought-vulnerable regions. A possible solution to the real-world problem is suggested in a way that the Los Angeles County Government or any possible stakeholders may consider intensive monitoring of the vulnerable hence at-risk regions introduced as half of the at-risk regions were found to be croplands or mountainous areas that are close to croplands. Though mountainous areas can create natural fire breaks due to elevation changes, however, Los Angeles County yet had many residential and agricultural areas on the edge of the mountainous areas within the wildfire-vulnerable regions, therefore intensive monitoring of those areas should be considered to prevent further agricultural damage hence economical loss but most importantly human casualties, worst-case scenario.

Appendix A: Additional Figures for Introduction



Figure A.1. Boundary of Los Angeles County, United States on Esri World Topographic Map

Table A.1. List of Landsat-8 Image Acquisition Dates

Image Acquisition Dates		
9 July 2022	1 July 2019	8 July 2016
6 July 2021	28 June 2018	20 June 2015
3 July 2020	11 July 2017	3 July 2014

Table A.2. Landsat-8 OLI Remote Sensing Spectral Index Formula

Landsat-8 OLI Spectral Indices	Formula
Normalised Difference Vegetation Index	$NDVI = \frac{NIR - RED}{NIR + RED} = \frac{\text{Band 5} - \text{Band 4}}{\text{Band 5} + \text{Band 4}}$
Land Surface Water Index	$LSWI = \frac{NIR - SWIR_1}{NIR + SWIR_1} = \frac{\text{Band 5} - \text{Band 6}}{\text{Band 5} + \text{Band 6}}$
Normalised Burn Ratio	$NBR = \frac{NIR - SWIR_2}{NIR + SWIR_2} = \frac{\text{Band 5} - \text{Band 7}}{\text{Band 5} + \text{Band 7}}$
differenced Normalised Difference Vegetation Index	$dNDVI = NDVI_{pre} - NDVI_{post}$
differenced Land Surface Water Index	$dLSWI = LSWI_{pre} - LSWI_{post}$
differenced Normalised Burn Ratio	$dNBR = NBR_{pre} - NBR_{post}$

Appendix B: Detailed Methodologies

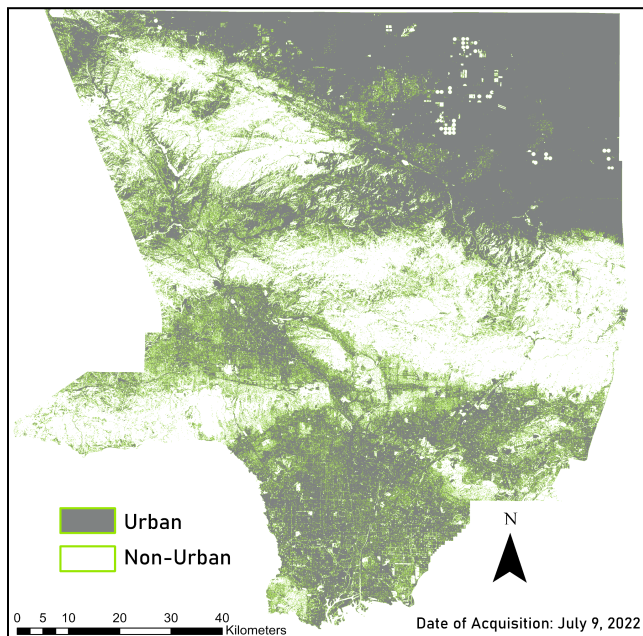


Figure B.1. Classified Image of 2022 Los Angeles County in Binary Output: Urban / Non-Urban

Table B.1. Classification Accuracy Assessment Report of 2022 Image

Table B.1(a). Error Matrix

Classified Data	Reference Data		
	Mountain/Ve	Urban/Resid	Row Total
Mountain/Ve	13	5	18
Urban/Resid	6	26	32
Column Total	19	31	50

Table B.1(b). Accuracy Totals

Class Name	Reference Totals	Classified Totals	Number Correct	Producer's Accuracy	User's Accuracy
Mountain/Ve	19	18	13	68.42%	72.22%
Urban/Resid	31	32	26	83.87%	81.25%
Totals	50	50	39		
<i>Overall Classification Accuracy</i>					78.00%

Table B.1(c). Kappa (K^{\wedge}) Statistics

Overall Kappa Statistics = 0.5283	
Conditional Kappa for each Category	
<i>Class Name</i>	<i>Kappa</i>
Mountain/Ve	0.5520
Urban/Resid	0.5066

References

- AGHAKOUCHAK, A., CHENG, L., MAZDIYASNI, O., and FARAHMAND, A., 2014, Global Warming and Changes in Risk of Concurrent Climate Extremes: Insights from the 2014 California Drought. *Geophysical Research Letters*, 41, pp. 8847–8852.
- DI BALDASSARRE, G., WANDERS, N., AGHAKOUCHAK, A., et al., 2018, Water Shortages Worsened by Reservoir Effects. *Nature Sustainability*, 1, pp. 617-622.
- MEDELLÍN-AZUARA, J., 2021, Economic Impacts of the 2020–22 Drought on California Agriculture. Available online at: https://cawaterlibrary.net/wp-content/uploads/2022/11/20AmSf-Economic_Impact_CA_Drought_V01.pdf (accessed 31 March 2023)
- STEPHENS, S. L., COLLINS, B. M., FETTIG, C. J., FINNEY, M. A., HOFFMAN, C. M., KNAPP, E. E., NORTH, M. P., SAFFORD, H., and WAYMAN, R. B., 2018, Drought, Tree Mortality, and Wildfire in Forests Adapted to Frequent Fire. *BioScience*, 68, pp. 77–88.
- TOKER, M., ÇOLAK, E., and SUNAR, F., 2021, Spatiotemporal change analysis of the protected areas: A case study – iğneada floodplain forests. *The International Archives of the Photogrammetry, Remote Sensing and Spatial Information Sciences*, XLIII-B3-2021, pp. 735–740.